# Analysis and Mitigation of The Lightning Overvoltage in Capacitively Coupling Grid Connected Offshore Wind Turbine

Mohamed A. Abouelatta, Mahmoud Ezzat*, M. A. Abd-Allah, and Abdelrahman Said

Power and Machine Department, Faculty of Engineering at Shoubra,
Benha University, Cairo, Egypt
*Mahmoud.selim@feng.bu.edu.eg

*Abstract:* Offshore wind turbines (OWT) are frequently struck by lightning, Because of their high constructions and the harsh marine environment. The high transient voltage from a lightning strike can cause huge damage to the devices of (OWT). In this paper a complete transient circuit model is established for the grid-connected offshore windfarm and an efficient analysis is also presented to evaluate the effect of changing the circuit parameters of blade, tower, grounding resistance, and lightning characteristics. Based on the circuit model, the transient voltage at the most sensitive points of the (OWT) can be determined during direct lightning strikes by ATP-EMTP and MATLAB software. Finally, mitigation techniques are investigated to reduce the overvoltage transients on an offshore wind turbine. This study used the GB50057-94 standard, as it stimulates the worst-case scenario especially in the regions with high lightning-strike probability. The results show that the use of the grounding wire is preferred as an active mitigation technique in offshore wind farms.

*Keywords*: Lightning strokes, offshore wind farm, overvoltage mitigation, ATP modelling.

## 1. Introduction

With the world's growing energy crisis, wind energy has emerged as one of the world's most rapidly produced and widely used renewable energy sources [1]. In case of offshore wind farms the sea environment is wet and rainy, the grounding environment is complex, lightning phenomena are frequent, and due to the tall structure of offshore wind turbines The risk of lightning strikes on (OWTs) has significantly increased [2]. The offshore wind turbine will be severely damaged by lightning, resulting in significant repair expenses including materials, labor, and downtime.

According to the statistics of the International Electro Technical Commission (IEC), lightning strikes cause up to 14% of wind power unit failures in places where lightning is common [3]. WTs are the most valuable components of wind farms, representing more than 60% of the total investment in wind power [1,2]. When a wind turbine is struck by lightning, the point struck delivers a massive quantity of energy to the lightning rod at the nacelle's rear [2,3]. The current goes through the blade's metal conductor, the engine room's guiding path, the tower body, and eventually into the WTs' grounding system. All elements of the wind turbine experience a potential rise as a result of this discharge process [4,5,6]. In this paper, the complete transient circuit model of practical 5MW ,690V/33 kV transformer connected to grid is built, A complete assessment of the blade, tower, and grounding resistance equivalent circuit parameters is also introduced. studying the transient voltage at different locations of the grid connected (OWT) during the direct lighting strike, and its mitigation techniques are proposed by ATP-EMTP and MATLAB software.

## 2. System description and modelling

The grid-connected offshore wind turbine under lightning strike is represented as shown in Figure 1 and can be described in two parts, the first one in the standalone wind turbine which is represented by the blade, tower, and grounding resistance stroked by lightning. the second part is the 690V wind turbine generator connected to 690 V/33 kV step-up transformer, the power is

Received: January 6th, 2021. Accepted: May 10th, 2022
DOI: 10.15676/ijeei.2022.14.2.12

transferred through a power cable which has mutual capacitance with the tower body then it connected to the 33/220 kV onshore step-up transformer through a XLPE submarine cable, this transformer is then connected to 220 kV grid system.

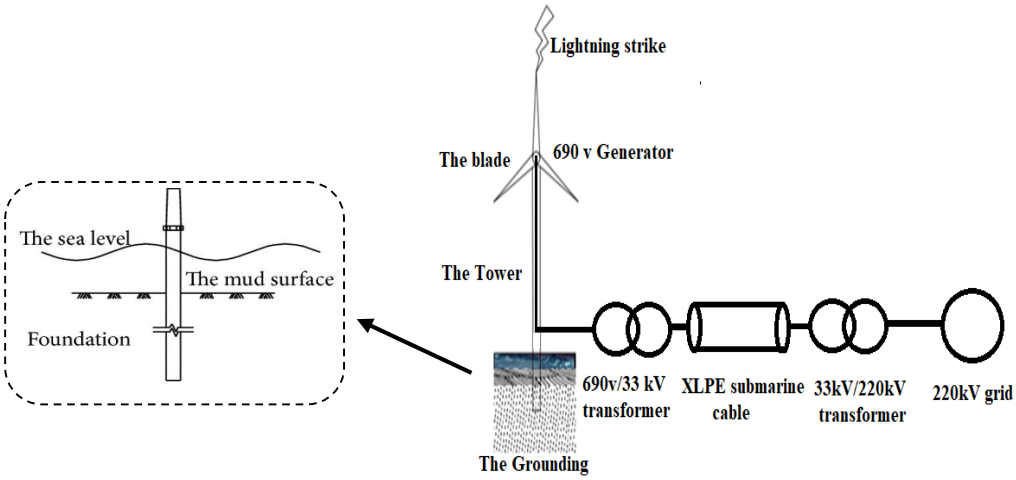


Figure 1. the system Layout including the layout of single pile foundation of the grounding system

## 3. System modelling

In this section, the transient model of Various parts of the grid-connected (OWT) is introduced and studying the factors affecting it.

*A. The Blade model*

To deal with the propagation wave phenomena of lightning current, the down conductor that is put within the blade to conduct the lightning current for transient analysis must be separated into a number of segments as shown in Figure. 2. Each segment can be represented as a π-circuit with resistance, inductance, and capacitance. [7]

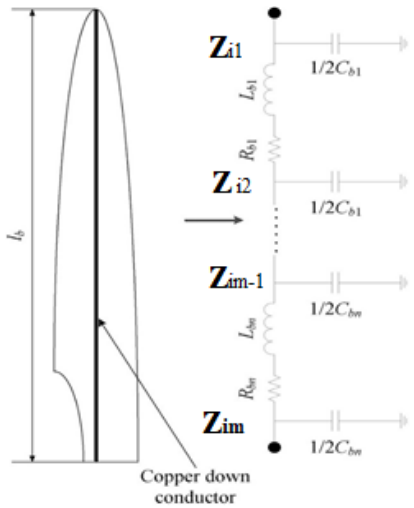


Figure 2. schematic diagram of the blade and down conductor, and the equivalent circuit model. [2]

The segment b length is taken as $L_b$=1.2m

$R_b =$

$$\rho \frac{L_b}{\pi r_b^2} \quad (1)$$

$$C_b = \frac{2\pi\varepsilon_0 L_b}{v_1+v_2} \quad (2)$$

$$V_1 = sinh^{-1}\left(\frac{\Delta L_b}{r_b}\right) - \frac{\sqrt{r_b^2+\Delta L_b^2}}{\Delta L_b} + \frac{r_b}{\Delta L_b} \quad (3)$$

$$V_2 = \frac{1}{\Delta L_b}\{z_{i1}sinh^{-1}\left(\frac{-2z_{i1}}{r_b}\right) + z_{i2}sinh^{-1}\left(\frac{-2z_{i2}}{r_b}\right) - (z_{i1}+z_{i2})sinh^{-1}\left[\frac{-(z_{i1}+z_{i2})}{r_b}\right] + \frac{1}{2}\sqrt{r_b^2+4z_{i1}^2} + \frac{1}{2}\sqrt{r_b^2+4z_{i2}^2} - \sqrt{r_b^2+(z_{i1}+z_{i2})^2} \quad (4)$$

$$L_b = \frac{\mu_0}{4\pi\Delta L_b}\{\Delta L_b \sinh^{-1}\left(\frac{L_b}{r_b}\right) - \sqrt{\Delta L_b^2 + r_b^2} + z_{i1}\sinh^{-1}\left(\frac{-2z_{i1}}{r_b}\right) + z_{i2}\sinh^{-1}\left(\frac{-2z_{i2}}{r_b}\right) - (z_{i1}+z_{i2})sinh^{-1}\left(\frac{-(z_{i1}+z_{i2})}{r_b}\right) + \frac{1}{2}\sqrt{r_b^2+4z_{i1}^2} + \frac{1}{2}\sqrt{r_b^2+4z_{i2}^2} - \sqrt{r_b^2+(z_{i1}+z_{i2})^2}\} \quad (5)$$

Where: $R_b$ , $C_b$, $L_b$ is the resistance [7], capacitance of segment b which can be calculated by the average potential method [8], and inductance of the segment b is calculated by the Neumann's integral formula respectively [9]. $\rho$ is the down conductor resistivity, $r_b$ is the down conductor radius, $L_b$ is the segment length, $z_{i1}, z_{i2}$ is the start and the end of the segment.

Blade wave impedance is affected by blade rotation angle as well as blade length, radius, and its material. Blade characteristics such as inductance and capacitance change when the blade rotates. As a result, according to the equations in [10,11], the correct blade wave impedance model must account for the effect of rotation angle.

The change in index of refraction and reflection between the blades and the tower is caused by this difference in inductance and capacitance. As a result, the current through the tower varies, and the transient potential peak of the nacelle varies. (OWTs) are most likely to be struck by lightning when the blade position is set to a, and the peak transient voltage of the (OWT) nacelle is at its maximum. This study simulates the worst case at position (a) as in Figure. 3.

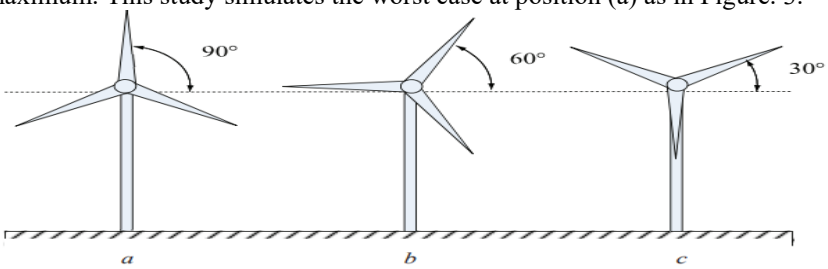


Figure 3. Three typical blade positions [10]

*B. The Tower model*

The actual tower of wind turbine is a hollow cone structure, so it can be modelled as a cylindrical shell as shown in the Figure 4(a).

The propagation wave phenomenon of lightning current going through the tower must be separated into segments, each of that is represented by a π -circuit as illustrated in Figure 4(b).

The segment resistance, inductance, capacitance can be calculated as:

$$R_t = \rho \frac{l_\tau}{s_T} \quad (6)$$

$$L_t = \frac{\mu_0 L_t}{2\pi}(\ln\frac{2L_t}{r_t} - 1 - \mu \ln c) \quad (7)$$

$$c_0 = 2\pi\varepsilon h_t / \ln\frac{h_t}{r_t} \quad (8)$$

Where: $s_t$ is the cross-section area of the conductor, $r_t$ is the outer radius of the conductor, $l_\tau$ is the length of the segment, C is the ratio between the inner and outer radius of the conductor, and $c_0$ is the total capacitance of the tower to ground, then the capacitance $c_i$ of each segment

can be calculated by the law of equal difference [12]. he inductance $L_t$ of the segment is calculated as [13].

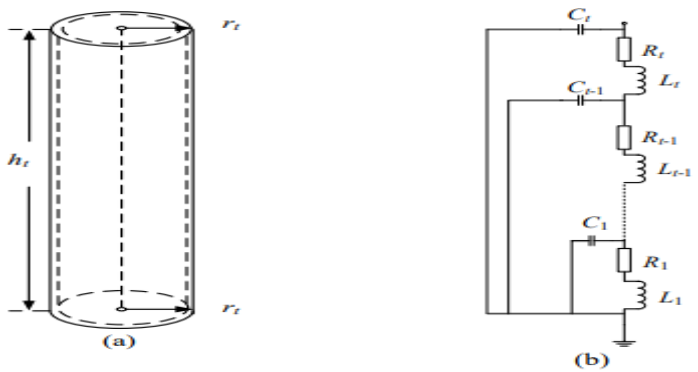


Figure 4. model of the tower. (a) schematic diagram of the cylindrical shell tower, (b) equivalent circuit model. [4]

*C. The lightning model*

The circuit model of the current source injected to the wind turbine is given in Figure 5 where $Z_0$ is the lightning channel impedance and its value (300Ω~400Ω) [4].

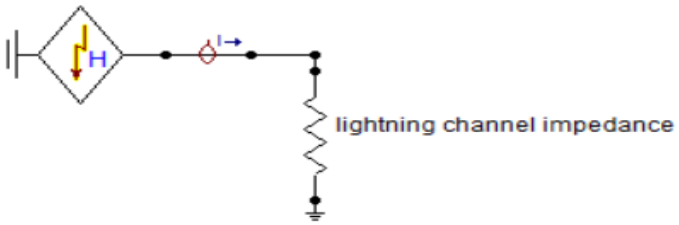


Figure. 5. the lightning current wave form

Heidler function is used to simulate lightning current waveform as shown in Figure.6 The mathematical expression of this function is [4,5]:

$$I(t)=\frac{Im}{\eta}\ \frac{(\frac{t}{\tau 1})}{1+(\frac{t}{\tau 1})\hat{}n}\ .\ e^{\frac{t}{\tau 2}} \qquad (9)$$

Where: Im is the peak value of lightning current; η is the lightning current correction factor, n is the lightning current steepness factor; τ1 is the front time constant, which is determined by the wave head time; τ2 is the delay time constant, which is determined by the tail time.

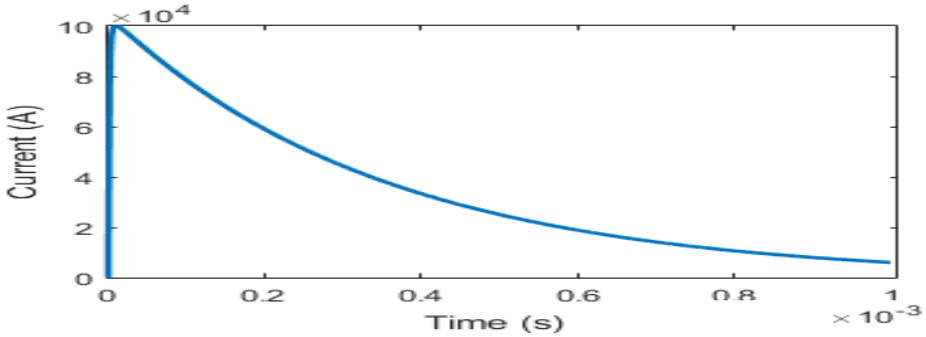


Figure. 6. the circuit model of the lightning current source

*D. Wind Turbine Generator*

Although a wind power generator includes a gearbox, synchronous or induction generator, rectifier, three-phase inverter, and other components, for the sake of this simulation, a stable synchronous generator is assumed. with line rms voltage of 690V, rated power of 5 MW, leakage reactance of 0.1H, and a frequency of 50 HZ.

*E. Transformer*

In order to model the transformer in a transient condition, the transformer model must include stray capacitance of the transformer coils. Although capacitances are scattered, lumped parameters for the total capacitance at the winding terminals can be employed with reasonable precision in this case. However, the transformer capacitances are often hard to be determined. Transformer capacitance is represented by CH, CL and CHL as shown in Figure. 7. Where, CH is the capacitance of high winding to ground, CL is the capacitance of low winding to ground and CHL is the capacitance between high and low windings. Normally the CL and CHL are greater than CH. This is because the fact that the high voltage calls for more separation between windings and between windings and core. These capacitances are shown in Table 1 [14].

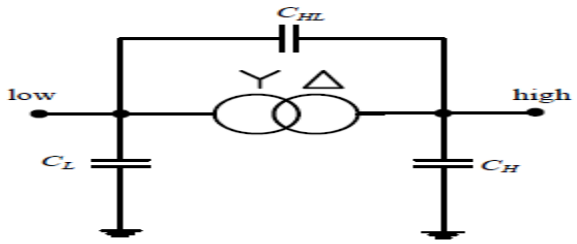


Figure. 7. High frequency transformer model

Table 1. Typical Capacitance of Transformers (Capacitance in nF) [13]

| Transformer MVA | Core Type | | |
|---|---|---|---|
| | CH | CHL | CL |
| 1 | 1.2-14 | 1.2-17 | 3.1-16 |
| 2 | 1.4-16 | 1-18 | 3-16 |
| 5 | 1.2-14 | 1.1-20 | 5.5-17 |
| 7 | 2.7-11 | 3.5-17 | 8-16 |
| 10 | 4-7 | 4-11 | 8-18 |
| 25 | 2.8-4.2 | 2.5-18 | 5.2-20 |

*F. XLPE Cable Modelling*

The EMTP-ATP simulation programme is unable to accurately depict all of the XLPE cables' characteristics and layers. practically, the cables' cores are designed to be segmented and stranded. There are also inner and outer semiconducting screens, as well as a sheath that could be mainly composed of a wire screen, making it hard to specify these conFigureurations directly in EMTP-ATP. In the cable's model, the cable constants are being combined through a conversion method considering the influence of stranded conductors, semiconducting layers, and sheath [15].

*I. Cable Core:*

The resistivity ρ and radius $r_1$ are required when providing core data. The core conductor, on the other hand, is frequently stranded, whereas CC routines assume a solid conductor. finally, To account for the gap between the strands, the resistivity of the core material must be increased using Equation (10). If the manufacturer has provided the DC resistance $R_{DC}$ of the core, the resistivity can be computed using Equation (11) [16].

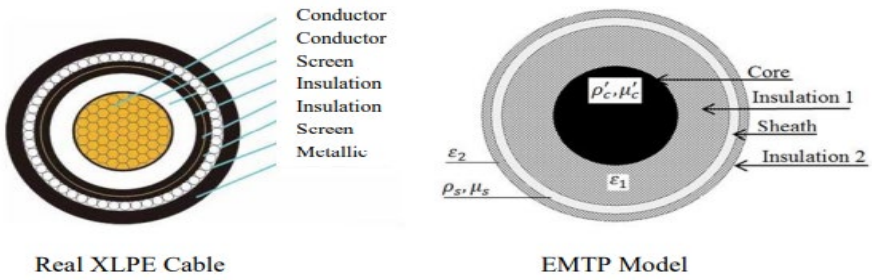


Figure 8. XLEP Cable model in EMTP-ATP

$$\rho_C = \rho * \frac{r_1^2 * \pi}{A_C} \quad (10)$$

$$\rho_C = R_{\mathrm{DC}} * \frac{r_1^2 * \pi}{A_C} \quad (11)$$

Gudmundsdottir, Unnur Stella, Et al illustrate that the resistance of the core cable can be calculated using either Equation (10) or Equation (11) because the slight difference between the two does not influence the simulation results' accuracy: The enhanced resistivity is $\rho c\ '$, the stranded core resistivity is $\rho$ , the nominal cross-sectional area of the core is Ac, and the radius of the core is $r_1$. $R_{DC}$= 0.0072 Ω/km, and $\rho c$ of annealed copper wires is 1.7241E-8 Ω·m, according to BS 60228 ,and $l$ is cable length per Km [19].

*II. Insulation and Semiconducting Screen:*

The cable's various semiconducting layers cannot be automatically included in the EMTP-ATP cable model. the influence of different semiconducting layers can be evaluated by Changing the electrical permittivity of the insulation while keeping the capacitance between the conductor and the metal screen constant, as given in Equation (12) [16].

$$\varepsilon = \varepsilon_r * \frac{ln\frac{r_2}{r_1}}{ln\frac{b}{a}} \quad (12)$$

Where $r_1$ is the core radius, $r_2$ is the sheath inner radius respectively, a and b are the inner and outer insulation radius respectively, and $\varepsilon_r$ is the permittivity of the insulating material ($\varepsilon_r$ = 2.3 for XLPE). This ignores any attenuation generated by semiconducting screens, which has an impact on the outcomes in case of very high frequency transient simulations.

*III. Inner Sheath:*

In this system we use ABB XLPE submarine cable its data is described in Table.2 [19].

Table 2. ABB XLPE submarine cable data

| | |
|---|---|
| Cross section of conductor (mm$^2$) | 95 |
| Diameter of conductor (mm) | 11.2 |
| Insulation thickness (mm) | 8.0 |
| Diameter over insulation (mm) | 29.6 |
| Cross section of screen (mm$^2$) | 16 |
| Outer diameter of cable (mm) | 104.0 |
| Cable weight (Copper) (kg/m) | 19.5 |
| Capacitance (μF/km) | 0.18 |
| Charging current per phase at 50 Hz (A/km) | 1.0 |
| Inductance (mH/km) | 0.44 |

Because a wire screen could not be specified in EMTP-ATP, the wire screen was replaced with a tubular conductor. The cross-sectional area of the tubular conductor is equal to the entire

wire area As. Equation (13) [16] can be used to compute the outer radius r3 of the tubular conductor if the inner sheath radius is r2. Figure. 8 is an ATP-EMTP model of a single core XLPE cable.

$$r_3 = \sqrt{\frac{A_s}{\pi}} * r_2^2 \tag{13}$$

## 4. Results and Discussion

After integrating all the equivalent circuit models described in the previous sections, a ATP-EMTP complete circuit model can be built for the grid connected offshore wind turbine, as shown in Figure.9 .When a lightning stroke with characteristics (maximum current of 100 KA, 10/350µs) hits the grid-connected offshore wind turbine with data described in Table.3 the overvoltage are obtained at the sensitive points which are the blade tip (A), the middle of the blade (B), the top of the tower (C), the middle of the tower (D), the terminals of the generator (E), the 33KV side of the grid-connected transformer (F), the grid terminals (G). these voltages are obtained at a grounding resistance Rg= 1Ω.

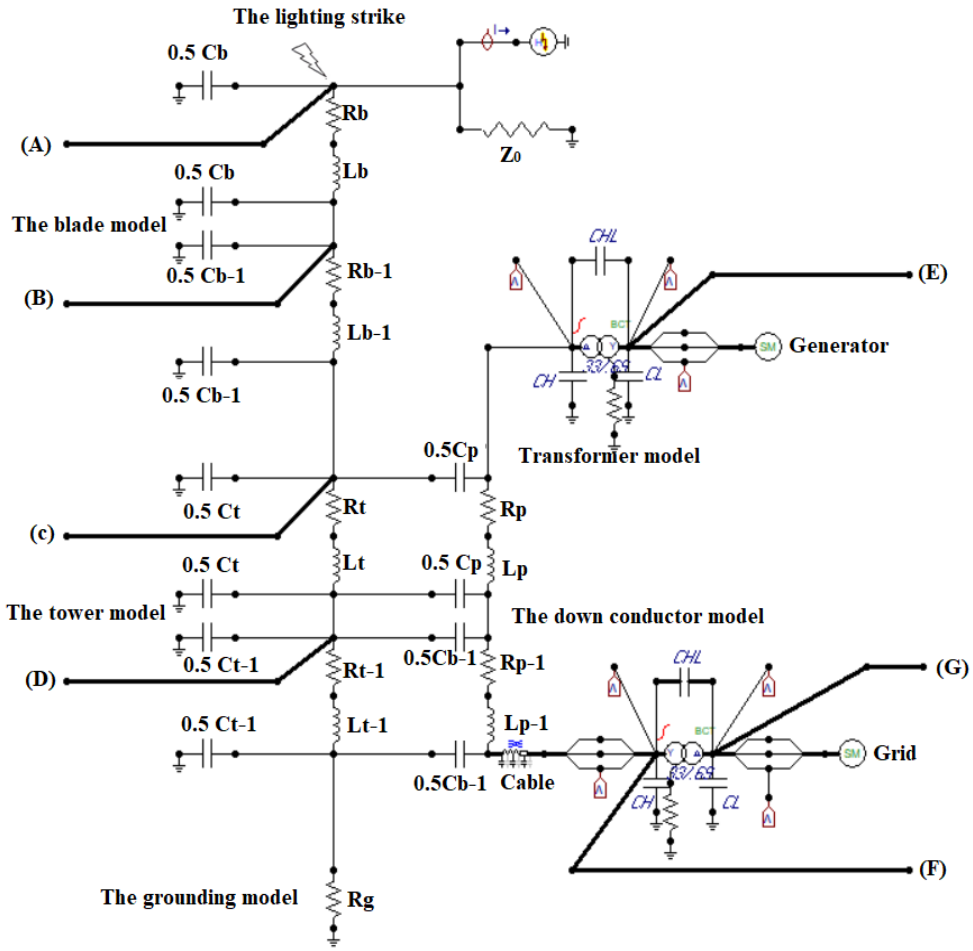


Figure 9. the complete equivalent circuit of grid connected offshore wind turbine

Table 3. Dimensions of an actual wind turbine

| | Parameters | Numerical values |
|---|---|---|
| Blade | Length /m<br>down conductor radius /mm | 50<br>4.7 |
| Tower | Height / m<br>Average thickness/mm<br>top dimeter /m<br>Down diameter / m | 70<br>46<br>3.52<br>4.8 |
| Jacket foundation | Seawater depth/m<br>Clay layer thickness /m seawater resistivity /Ω.m<br>Clay resistivity/ Ω.m<br>Ravel resistivity/ Ω.m | 10<br>15<br>1<br>150<br>1000 |

*A. Overvoltage at more sensitive points*

The overvoltage at the more sensitive points of grid connected offshore wind turbine under lightning stroke is calculated and analysed. Figure.10 and Figure.11 show that the transient overvoltage reaches very high values such that, 9.34 MV at point (A), 4.54 MV at point (B), which are a sufficient value to get the blade damage. and 1.5 MV at point (C) which is the nacelle voltage it is large enough to affect badly on the performance of the control room including the generator, control, and protective devices. Also, it reaches 795 kV at point (D), 13 kV at point (E), 330 kV at point (F), and 395 kV at point (G). With comparing these values with the BIL, shown in Figure.10, it is clear that these values is large enough to damage the wind turbine transformer.

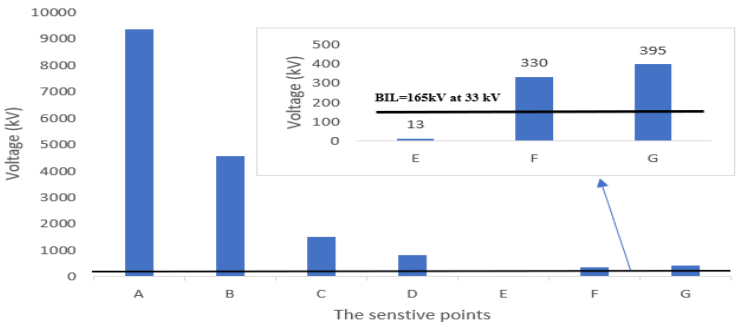


Figure. 10. comparing the overvoltage values to BIL at 33 KV

Also, the waveforms in Figure. 11 and Figure. 12 have obvious oscillations, this behaviour is attributed to the existence of the inductances and capacitances in the circuit model, and the reflection and refraction effects of the travelling waves. The transient potentials are calculated in different distances on the blade (point A, B) as shown in Figures.10 (a) and (b), so that the potential gradient and creeping discharge can be assessed and finally a reasonable distance between the receptors can be chosen to avoid the creeping discharge and the thermal damage to the blades. Also, the transient potentials are calculated in different distances on the tower (point C, D) as shown in the Figures.10 (c) and (d) to choose the safe distance to avoid the backflash which may damage the facilities inside the tower [4,5].

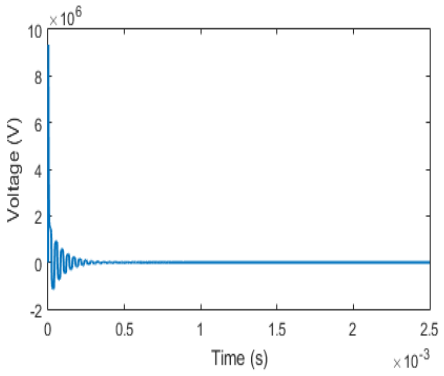


*(a) the* overvoltage *at point (A)*

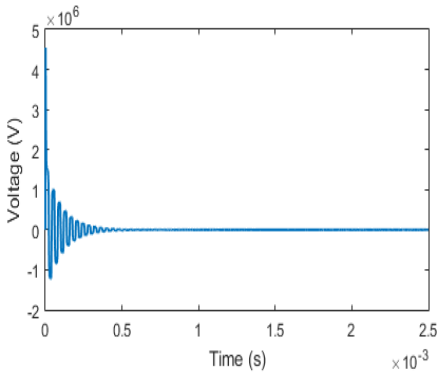


(b) the overvoltage at point (B)

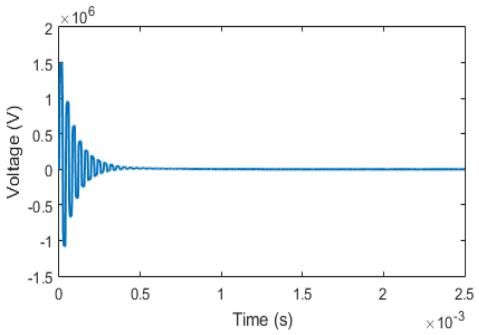


(c) the overvoltage at point (C)

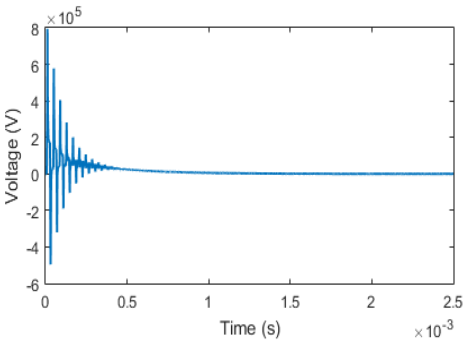


(d) the overvoltage at point (D)

Figure. 11. the overvoltage at the sensitive points A, B, C, D

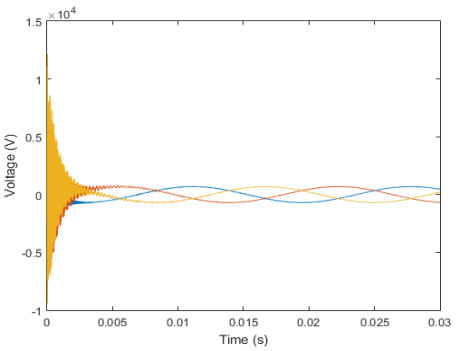


(a) the overvoltage at point (E)

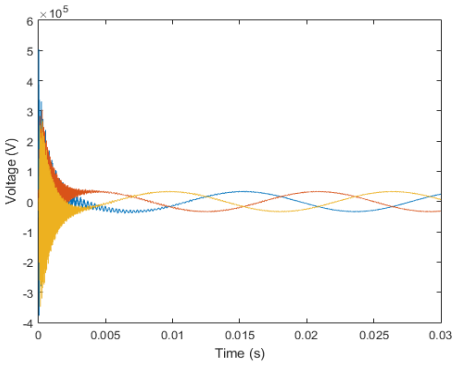


(b) the overvoltage at point (F)

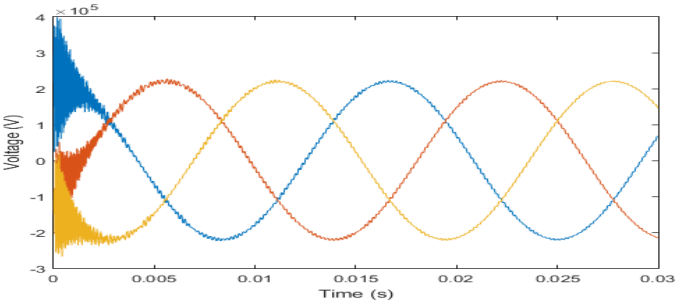


(c) the overvoltage at point (G)

Figure 12. the overvoltage at the sensitive points E, F, G

*B. The effective factors on the grid connected offshore wind turbine overvoltage.*

This section demonstrates the effect of the various factors on the transient overvoltage on grid-connected offshore wind turbine.

*B.1. lightning parameters*

The peak value of the lightning stroke, the wave front and the wave tail time are the main parameters of the lightning current waveform. Different lightning current waveforms with different values of peak, front and tail times, to get the peak transient potential, and the speed of the transient overvoltage decay at the sensitive points (A, B, C, D, E, F, G).

A-The peak value effect

When a lightning strike hits the grid-connected offshore wind turbine with different peak current (50 kA.63 kA,100 kA), while the front and tail time are constant (10/350 μs), the peak transient potential and the speed of the transient overvoltage decay time at the points (A,B,C,D,E,F,G) is obtained in Table.4.

It's clear that, as the peak of the lightning current increase the peak transient voltage is also increased at the different locations along the wind turbine. Also, it has almost no effect on the decay time of the wave at each single point, but it takes longer time to decay while moving from the blade tip to the bottom of the tower. It can be explained as the propagated wave has more chance to reflect and refract along the body of the turbine as the distance increase, so it takes more time to decay [18].

*B-front time and tail time characteristics effect*

The influence of the changing of the front time with values (1.2 μs ,2.6 μs, 10 μs) and tail time with values (50 μs, 100 μs, 350μs) with constant peak lightning current of 100 kA is studied in this section. the peak transient potential and the speed of the transient overvoltage decay at the points (A, B, C, D, E, F, G) is obtained in Table.5 and Table.6.

It's concluded that from table.5, as the wave front time decreased the peak of the transient potential increased significantly which can be explained as follows, the overall impedance of the wind turbine is perceptive, so the voltage value in the nacelle is available in equation(14) [20].

$$u = L\frac{di}{dt} + \mathrm{i}R \tag{14}$$

where L is the wind turbine equivalent inductance, R is the wind turbine equivalent resistance, i is the lightning current. di/dt is the sum of the changes of the lightning flow itself and the variation of the current reflection. As a result, the wave front time has a significant impact on the transient process of the offshore wind turbine's lightning stroke. Because the wave front time is significantly shorter than the tail time, when the wave front time drops, the high frequency component rises and the di/dt value rises, the peak transient potential value rises as well. Table.6 shows that as the wave tail time increase the peak transient potential also increase because the wave take much time to decay to its half value after reaching its peak so that the propagated waves have more chance to accumulated making the voltage to increase [19]. The results also show that whether changing the front time or the tail time it has almost no effect on the decay time.

Table 4. the peak value effect

| Lightning current peak (KA)(10/350) µs | Peak voltage in (MV) | | | | | | | Decay time in (ms) | | | | | | |
|---|---|---|---|---|---|---|---|---|---|---|---|---|---|---|
| | A | B | C | D | E | F | G | A | B | C | D | E | F | G |
| 50 | 4.44 | 2.35 | 0.753 | 0.750 | 0.064 | 0.250 | 0.304 | 0.45 | 0.64 | 0.71 | 0.82 | 0.51 | 0.41 | 0.43 |
| 63 | 5.6 | 2.91 | 0.948 | 0.773 | 0.079 | 0.320 | 0.330 | 0.49 | 0.67 | 0.73 | 0.84 | 0.53 | 0.47 | 0.47 |
| 100 | 9.34 | 4.54 | 1.5 | 0.795 | 0.013 | 0.330 | 0.395 | 0.5 | 0.68 | 0.74 | 0.85 | 0.6 | 0.5 | 0.5 |

Table 5. Front time effect

| Wave characteristics (100kA) | Peak voltage in (MV) | | | | | | | Decay time in (ms) | | | | | | |
|---|---|---|---|---|---|---|---|---|---|---|---|---|---|---|
| | A | B | C | D | E | F | G | A | B | C | D | E | F | G |
| 1.2/350 µs | 18.6 | 8.66 | 1.53 | 1.43 | 0.02 | 0.349 | 0.4 | 0.37 | 1.1 | 0.91 | 0.92 | 0.4 | 0.4 | 0.4 |
| 2.6/350 µs | 18.3 | 8.52 | 1.52 | 1.42 | 0.020 | 0.339 | 0.398 | 0.49 | 1.2 | 0.86 | 0.85 | 0.5 | 0.4 | 0.4 |
| 10/350 µs | 9.34 | 4.54 | 1.5 | 0.795 | 0.013 | 0.33 | 0.395 | 0.5 | 0.68 | 0.74 | 0.85 | 0.6 | 0.5 | 0.5 |

Table 6. Tail time effect

| Wave characteristics (100kA) | Peak voltage in (MV) | | | | | | | Decay time in (ms) | | | | | | |
|---|---|---|---|---|---|---|---|---|---|---|---|---|---|---|
| | A | B | C | D | E | F | G | A | B | C | D | E | F | G |
| 10/50 µs | 5.86 | 2.98 | 1.5 | 1.29 | 0.083 | 0.31 | 0.398 | 0.45 | 0.54 | 0.56 | 0.61 | 0.5 | 0.4 | 0.4 |
| 10/100 µs | 6.88 | 3.4 | 1.51 | 1.36 | 0.01 | 0.32 | 0.397 | 0.49 | 0.53 | 0.54 | 0.54 | 0.4 | 0.4 | 0.4 |
| 10/350 µs | 9.34 | 4.54 | 1.5 | 0.795 | 0.013 | 0.33 | 0.395 | 0.5 | 0.68 | 0.74 | 0.85 | 0.6 | 0.5 | 0.5 |

*C-Lightning standard waveform effect*

The lightning current waveforms characteristic used in the previous section were standard and non-standard waveforms to show, generally, the effect of the front and tail times on the peak transient overvoltage and its decay time.

Table.7 shows the waveform characteristic according to different standards. The transient overvoltage at the blade tip is computed under these standard waveforms taken the peak lightning current 100 kA at all standards. It is clear from Figure.13 that the GB50057-94 standard, and The Egyptian standard simulate the worst-case scenario as the overvoltage reaches 18.54 MV, and 18.32 MV respectively, then DL/T620-1997 which has 16.76 MV peak value, and finally IEC61312 with 9.43 MV. This can be attributed to, the sm aller the wave front, the higher transient overvoltage at the different points as explained in the previous section. So, it is recommended to study the overvoltage transient and design the mitigation and protective devices with the standard which has a small wave front like (GB50057-94, The Egyptian standard) as it simulates the worst-case scenario specially in the regions with high

lightning strike probability.

Table.7 standard lightning current waveforms

| Standards | Waveform characteristic |
|---|---|
| DL/T620-1997 | 2.6/50 µs |
| GB50057-94 | 0.25/100 µs |
| IEC61312 | 10/350 µs |
| The Egyptian code | 1/50 µs |

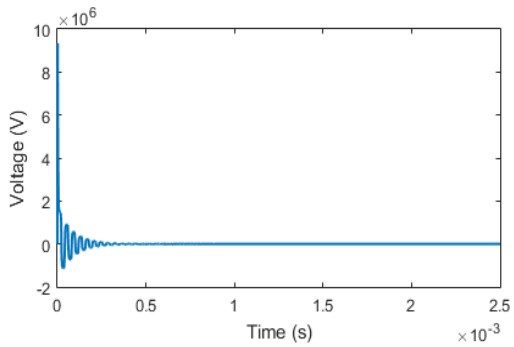


(a) the bade tip voltage according to DL/T620-1997

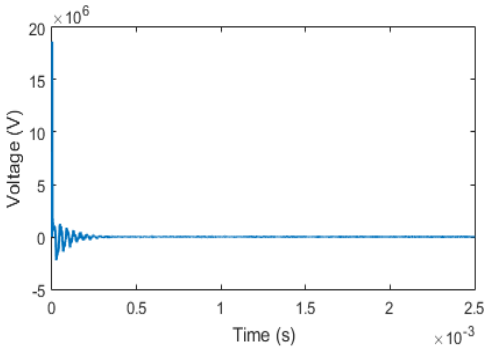


(b) the bade tip voltage according to GB50057-94

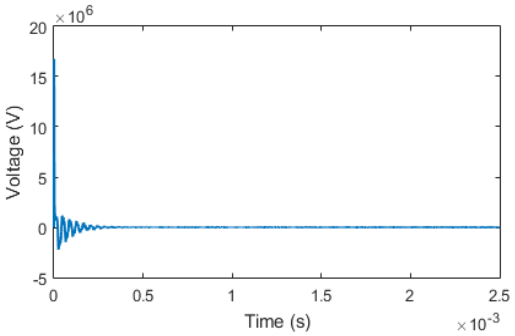


(c) the bade tip voltage according to IEC61312

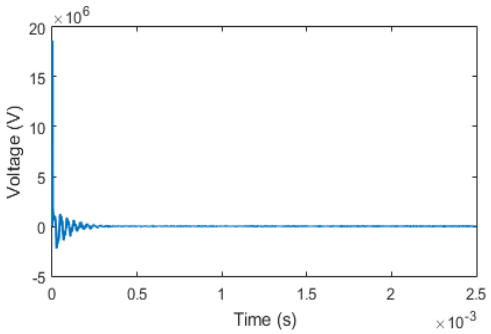


(d) the bade tip voltage according to Egyptian code

Figure 13. the bade tip voltage according to DL/T620-1997, GB50057-94, IEC61312 standard, and Egyptian code

*B.2 Blade length and tower height*

In this section, the influence of changing the tower height with values (70 m, 85m) at constant blade length of 50 m, and the changing of the blade length with values (50m, 60m) with constant tower height of 70m were investigated. The results were shown in Table.8, and Table.9. The results show that the nacelle voltage (C) is the most sensitive point to the change of the tower height or the blade length, it reaches to about 1.5 MV and 3.2 MV at tower length of 70m and 85 m respectively. The voltage at point C is increased as the height of the tower increased as a result of increasing the channel impedance of it. On the other hand, the voltage at point (C) reaches about 1.5 MV and 1.1 MV at blade length of 50m and 60 m respectively. The voltage at point (C) is decreased with the increasing of blade length as the voltage drop on blade is increased with increasing in its length. So, it is concluded that a higher tower and shorter blades will increase the probability of the damage in the nacelle [19].

Table 8. Tower height effect

| Blade length(m) | Tower height (m) | Peak voltage in (MV) | | | | | | |
|---|---|---|---|---|---|---|---|---|
| | | A | B | C | D | E | F | G |
| 50 | 70 m | 9.34 | 4.54 | 1.5 | 0.795 | 0.013 | 0.33 | 0.395 |
| 50 | 85 | 9.13 | 4.72 | 3.2 | 1.76 | 0.125 | 0.335 | 0.41 |

Table 9. Blade length effect

| Blade length(m) | Tower height (m) | Peak voltage in (MV) | | | | | | |
|---|---|---|---|---|---|---|---|---|
| | | A | B | C | D | E | F | G |
| 50 | 70 | 9.34 | 4.54 | 1.5 | 0.795 | 0.013 | 0.33 | 0.395 |
| 60 | 70 | 9.7 | 5.1 | 1.1 | 0.61 | 0.015 | 0.342 | 0.412 |

**5. Lightning transient overvoltage mitigation techniques**

The lightning stroke, as seen, generates a very high transient potential at the sensitive points, where the huge energy associated with these transients can destroy the turbine or take it out of service. So, a mitigation technique must be used to reduce these high potentials at the different sensitive points to protect them from damage.

*A. Grounding resistance*

Offshore wind turbines are grounded using foundation grounding. Single pile foundations, gravity foundations, suction foundations, tripod foundations, and suspension foundations are all common types [21]. Single-pile type grounding is the most common, accounting for more than 65% of all basic grounding. Figure.14 shows a schematic representation of the single pile foundation structure [15].

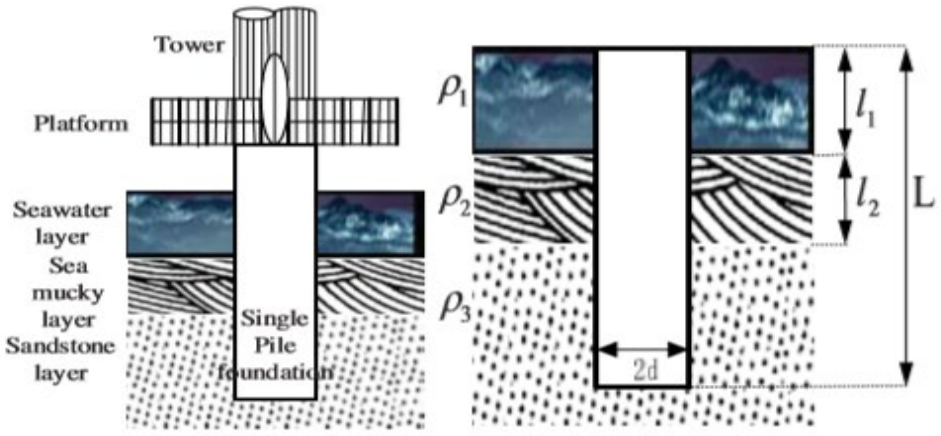


Figure 14. Single piled foundation of offshore wind turbine Schematic diagram and grounding of offshore wind turbine in the intertidal zone [5]

The expression of the impact grounding resistance of a single pile wind turbine in intertidal grounding environment is obtained [23,24,25]:

$$R=\frac{\alpha\,\rho_{1,2eq}\,\rho_3}{2\pi[\rho_3(L_1+L_2)+\rho_{1,2eq}(L-L_1-L_2)]}\left[\ln\frac{L+\sqrt{d^2+L^2}}{d}\sum_{n=0}^{\infty}k^n\ln\frac{2n(L_1+L_2)+L+\sqrt{d^2+[2n(L_1+L_2)+L]^2}}{2n(L_1+L_2)-L+\sqrt{d^2+[2n(L_1+L_2)-L]^2}}\right] \quad (15)$$

Where:

α: is the impulse factor and its approximate value = 1

K: is the soil reflection coefficient, K=$(\rho_3-\rho_{1,2eq})/(\rho_3+\rho_{1,2eq})$

$\rho_1$: the resistivity of seawater layer

$\rho_2$: the resistivity of silt layer

$\rho_{1,2eq}$: the equivalent soil resistivity of the seawater layer and the silt layer
$\rho_3$: the resistivity of sandstone layer
$L_1$: depth of seawater layer
$L_2$: depth of silt layer
L: the length of the grounding foundation extending into sand
d: the radius of the grounded foundation

*A- Influence of sandstone layer's resistivity*

The effect of the resistivity of the sandstone layer located under the sea water on the grounding resistance is presented and discussed in this section.

As shown from Figure.15 the impact grounding resistance has a noticeable increase with the increase of the resistivity of the sandstone layer at low seawater depth like 0 m, and 0.5 m, but as the depth increase the resistivity of the sandstone layer has almost no effect on the impact grounding resistance.

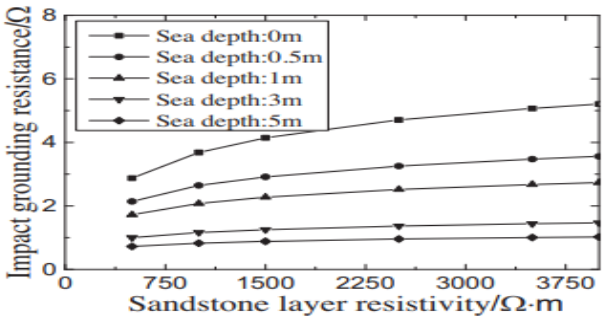


Figure 15. the change of the grounding resistance with the sandstone resistivity in terms of the sea water depth

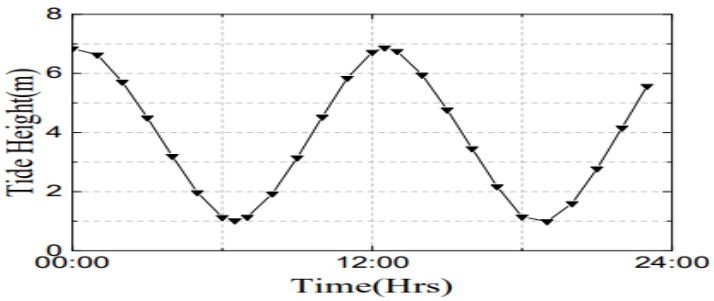


Figure. 16. the tide height variation over time

*B- Influence of Depth of Seawater Layer*

The variation of seawater depth caused by tidal wave is an important factor affection the grounding resistance of intertidal zone wind turbine. Figure.16 shows how the seawater layer changed over time.

The Figure shows that the seawater layer fluctuates between 0 and 7 meter. Equation (15) is used to evaluate the variation of the grounding resistance with the seawater layer. The parameters were taken as follow:$\rho_1$=5, $\rho_2$=60, $\rho_3$=1500 ohm. $L_2$=10m, L=20m, d=2.5 m, so we can find how the grounding resistance changes with the seawater depth.

The impact grounding resistance of an intertidal zone wind turbine drops significantly as the depth of the sea layer increases, as shown in Figure.17. It decreases from 6Ω at 0 m to 0.66Ω at 7 m.

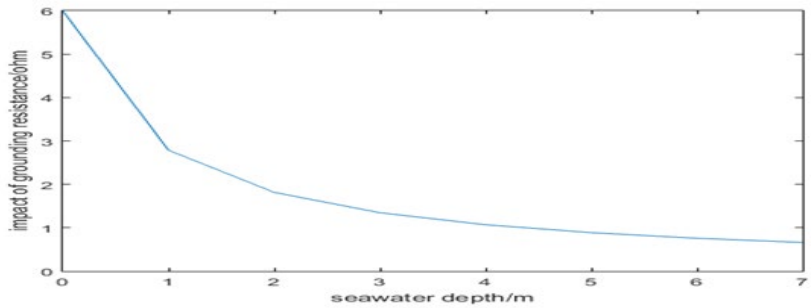


Figure. 17. the effect of sea water depth on the grounding resistance

As mentioned in section 5.1 The grounding resistance of the offshore wind turbine is found to be changed from 0.66Ω to 6Ω, Figure.18, Figure.19 and Figure.20, show the voltages that appear at the sensitive points (A, B, C, D, E, F, G) of the system at the minimum and maximum grounding resistance Rg=0.66Ω and Rg=6Ω respectively.

The results show that the grounding resistance value has almost no effect on the overvoltage value, on the other hand it has a significantly effect in the overvoltage oscillations, The harmonic content of the overvoltage at the blade tip was analysed using FFT (Fast Fourier Transform), the harmonic spectrum in the two cases is shown in Figure.17 (c, d), the THD is decreased to 130.21%, compared to 650.33% at Rg=0.66Ω.

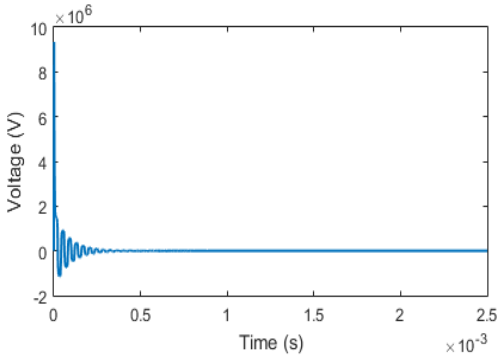


(a) O.V at point (A) at Rg=0.66Ω

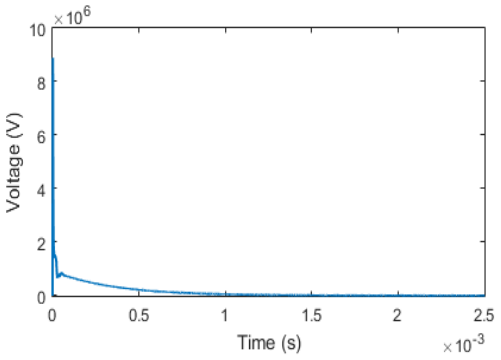


(b) O.V at point (A) at Rg=6Ω

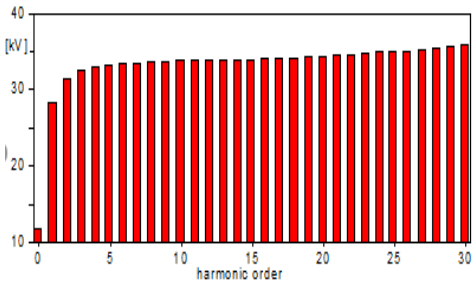


(c) Harmonic spectrum at point (A) at Rg=0.66Ω

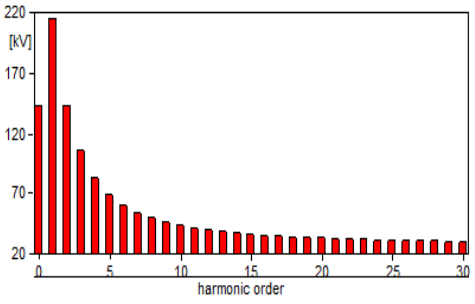


(d) Harmonic spectrum at point (A) at Rg=6Ω

Figure. 18. The overvoltage and harmonic spectrum at point A at minimum and maximum grounding resistance

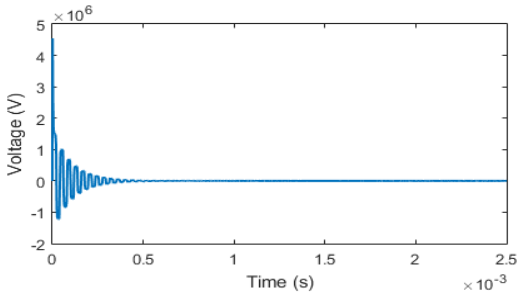


(a) O.V at point (B) at Rg=0.66Ω

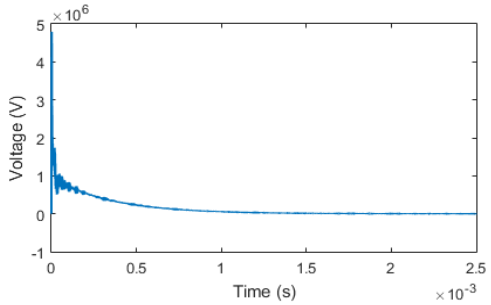


(b) O.V at point (D) at Rg=6Ω

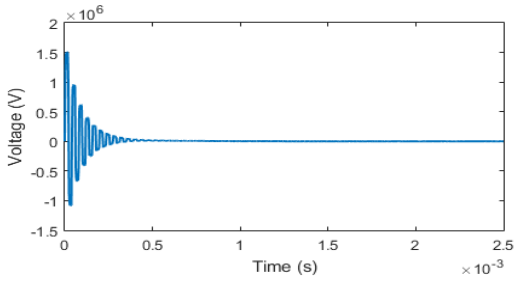


(c) O.V at point (c) at Rg=0.66Ω

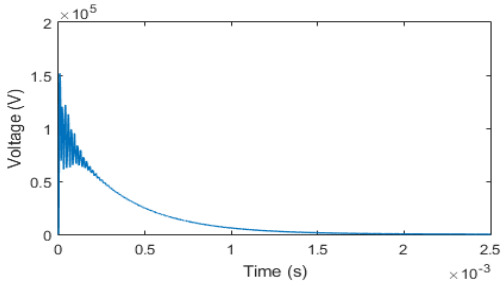


(d) O.V at point (c) at Rg=6Ω

Figure. 19. The overvoltage at points B,C at minimum and maximum grounding resistance

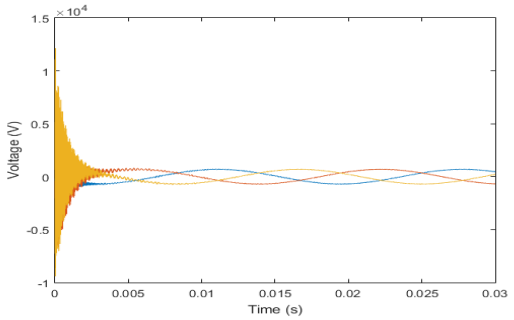


(a) O.V at point (E) at Rg=0.66Ω

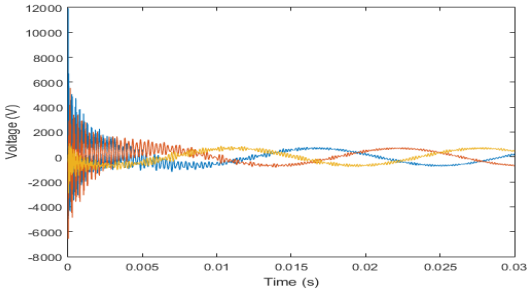


(b) O.V at point (E) at Rg=6Ω

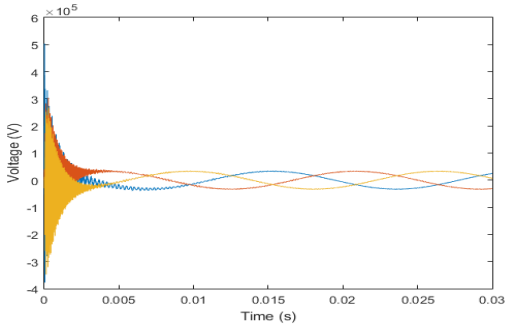


(c) O.V at point (F) at Rg=0.66Ω

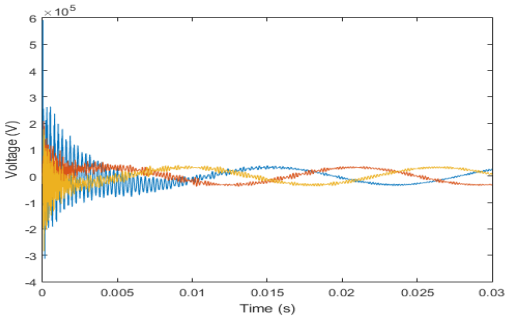


(d) O.V at point (F) at Rg=6Ω

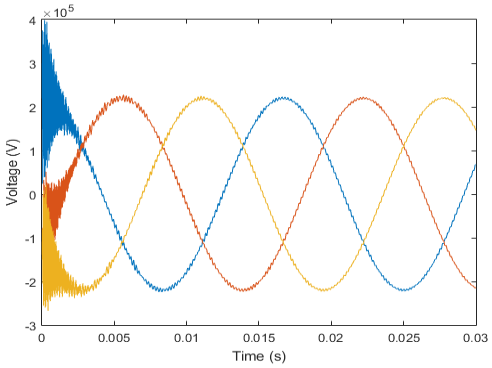


(e) O.V at point (G) at Rg=0.66Ω

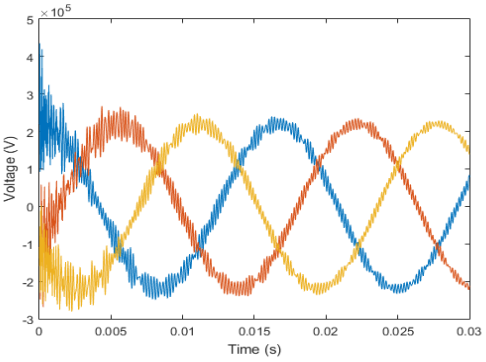


(f) O.V at point (G) at Rg=6Ω

Figure. 20. The overvoltage at points E, F, G at minimum and maximum grounding resistance

*B. Grounding wire*

In this section, the effect of Connecting a ground wire from the nacelle to the grounding system on the overvoltage happen on the sensitive points (A, B, C, D, E, F, G) is presented and analysed. Figure.21, Figure.22, and Figure.23 show a significantly decrease in the values of the peak transient voltages and also overvoltage oscillations as compared with the values without the grounding wire. The results are summarized in Table.10.

It's clear that the voltage at all the sensitive points have a significant decrease, especially the value of the peak transient voltage at the top of the tower (nacelle voltage) as the grounding wire is connecting from this point it provides an alternative path to the lightning current because it has a smaller impedance, so most of the current is directed to this path to be discharged in the ground. also, the potential gradient is decreased between that points so that the creeping discharge and thermal damage can be avoided. So, it provides more safety for the engine room and the facilities inside the tower.

Table 10. comparison between the transient O.V with and without the grounding wire

| The peak overvoltage | Without grounding wire | With grounding wire |
|---|---|---|
| The peak overvoltage at point (A) | 9.34 MV | 8.55 MV |
| The peak overvoltage at point (B) | 4.54 MV | 4.12 MV |
| The peak overvoltage at point (C) | 1.5 MV | 151 kV |
| The peak overvoltage at point (D) | 795 kV | 150.47 kV |
| The peak overvoltage at point (E) | 13 kV | 4.5 kV |
| The peak overvoltage at point (F) | 330 kV | 57 kV |
| The peak overvoltage at point (G) | 395 kV | 230 kV |

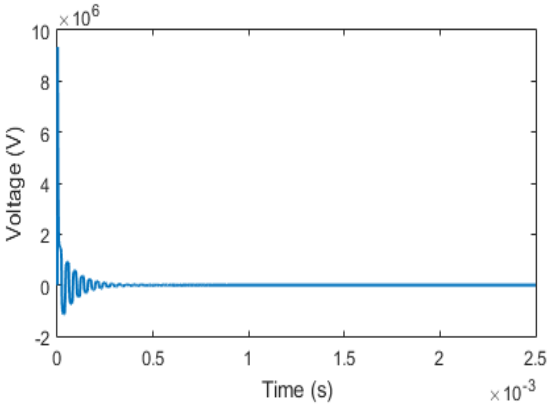


(a) O.V at point (A) Without grounding wire

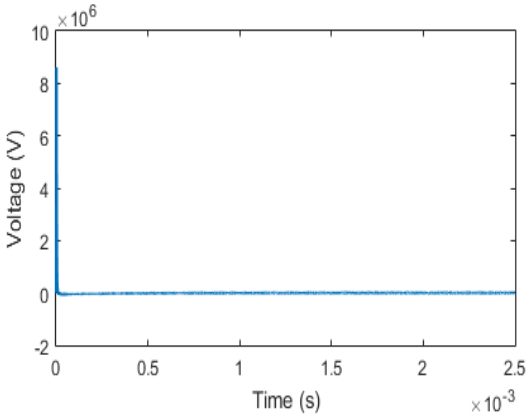


(b) O.V at point (A) With grounding wire

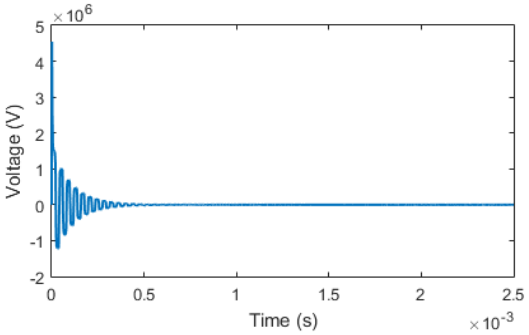


(c) O.V at point (B) Without grounding wire

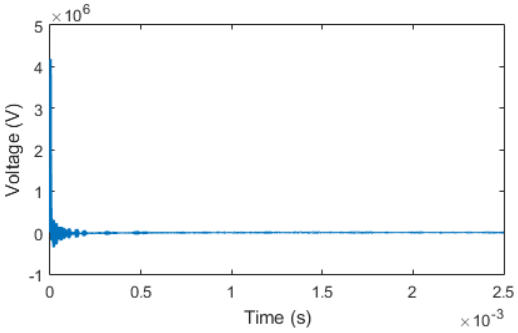


(d) O.V at point (B) With grounding wire

Figure. 21. The overvoltage at points A,B with and without the grounding wire

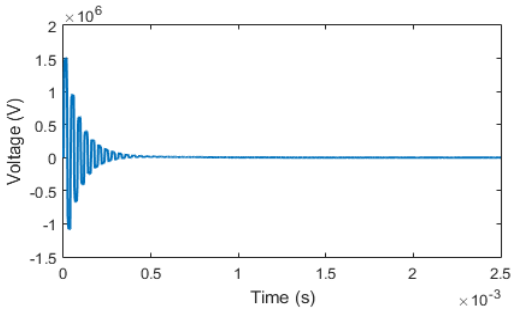


(a) O.V at point (c) Without grounding wire

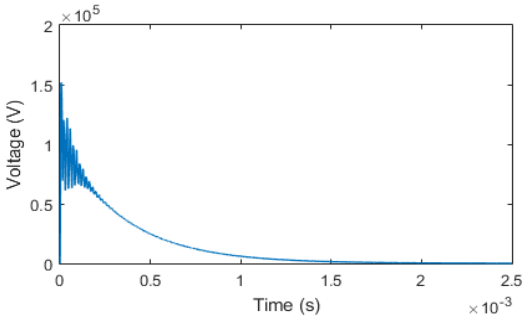


(b) O.V at point (c) With grounding wire

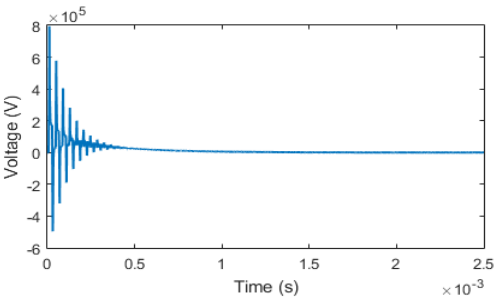


(c) O.V at point (d) Without grounding wire

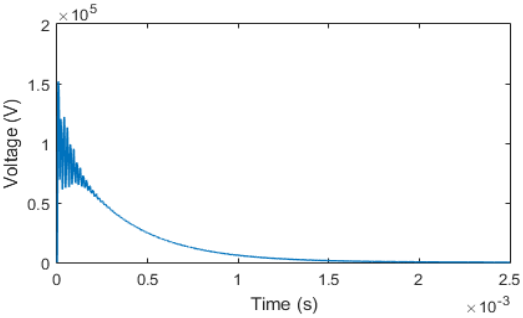


(d) O.V at point (d) With grounding wire

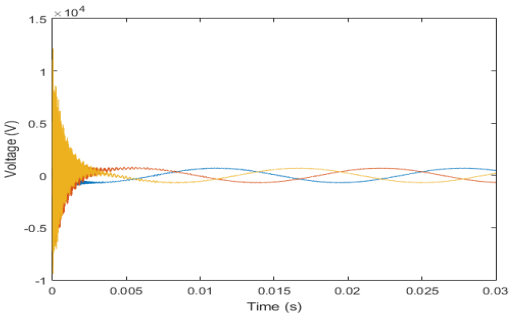


(e) O.V at point (E) Without grounding wire

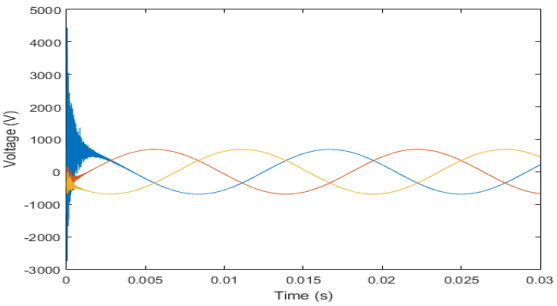


(f) O.V at point (E) With grounding wire

Figure. 22. The overvoltage at points C, D, E with and without the grounding wire

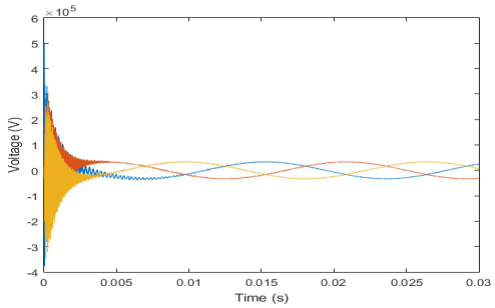


(a) O.V at point (F) Without grounding wire

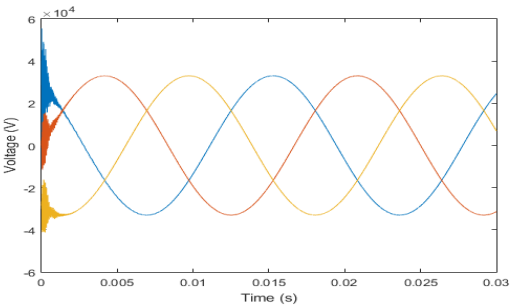


(b) O.V at point (F) With grounding wire

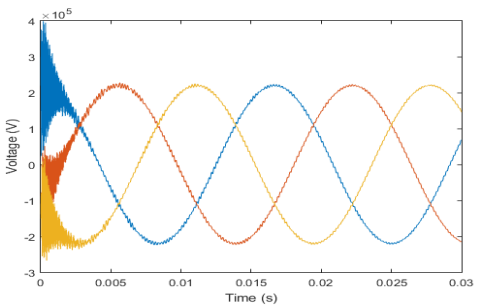


(C) O.V at point (G) With grounding wire

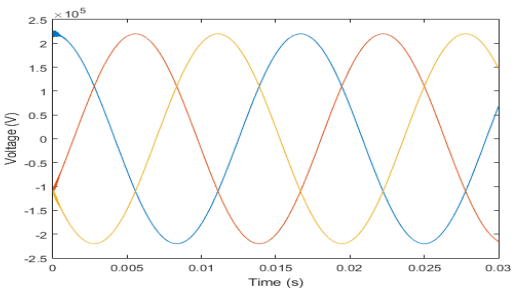


(d) O.V at point (G) With grounding wire

Figure. 23. The overvoltage at points F,G with and without the grounding wire

**6. Conclusion**

1. In this paper the ATP-EMTP transient model of the 5MW,690V/33 kV grid – connected offshore wind turbine is proposed, the factors affecting the peak transient voltage at the sensitive points of the system, and its decay time are analysed, finally mitigation techniques are investigated to reduce the peak transient voltage. The work is performed using ATP-EMTP and MATLP software. The following can be concluded:
2. The wave front time is the most effective factor on the peak transient overvoltage. As the front time decreases, the induced voltages at different sensitive points increased. So, the standard waves used by GB50057-94 standard and the Egyptian standard represents the worst-case scenario. The peak induced overvoltage reaches about 18.54MV, and 18.32 MV with using GB50057-94, and the Egyptian standards respectively, and reaches to about 16.76 MV, and 9.43 MV for DL/T620-1997 and IEC61312 standards respectively.
3. The peak overvoltage at the nacelle increases from 1.5 MV to 3.2 MV when the tower height increased from 70m to 85m, with constant blade length. On the other hand, the peak

overvoltage increased from 1.5 MV to 1.1 MV when the blade length increased from 50m to 60m. respectively, which lowered the probability of damage to the nacelle and the control room.

4. It is not recommended to use the grounding resistance as a mitigation technique in offshore wind farms unlike the onshore wind farms, as
5. The results showed that the grounding resistance value has almost no effect on the peak transient overvoltage, but it has a great effect on overvoltage waveform oscillations. The peak overvoltage at the blade tip has almost no change when the grounding resistance change from 0.66Ω to 6 Ω, but the THD decreases significantly from 650.33% to 130.21%.
6. Using a ground wire as a mitigation technique shows a high efficiency in reducing the induced overvoltage. The peak overvoltage reduces by 8.5%, 5.07%, 87.1%, 66.4%, 65.3 %, 82.7%, and 41.7% at the points (A, B, C, D, E, F, G) respectively. Also, the THD at point A decreases to 53.12% comparing with 650.33% without using the grounding wire.

## 7. References


[1]. Chang, Yuan, et al. "Risk assessment of generation and transmission systems considering wind power penetration." 2018 *International Conference on Power System Technology (POWERCON). IEEE*, 2018.

[2]. Zhang, Jie, et al. "The impact of lightning strike to multi-blade on the lightning overvoltage and stresses of arresters in offshore wind farm." *IET Renewable Power Generation* 15.13 (2021): 2814-2825.

[3]. Xiang, Xiao, Zhang Xiaoqing, and Li Cong. "Simulation analysis on overvoltage in wind turbines by lightning stroke." *Transactions of China Electrotechnical Society* 30.24 (2015): 237-244.

[4]. Tao, Shiqi, et al. "Research of lightning transient potential on the jacket foundation offshore wind turbines." *E3S Web of Conferences*. Vol. 95. EDP Sciences, 2019.

[5]. Heng, Lu, et al. "Modeling of Offshore Wind Turbine Under Lightning Stroke and Analysis of Impact Factors on Transient Overvoltage." 2019 11th *Asia-Pacific International Conference on Lightning (APL). IEEE*, 2019.

[6]. Yamamoto, Kazuo, et al. "An experimental study of lightning overvoltages in wind turbine generation systems using a reduced-size model." *Electrical Engineering* in Japan 158. 4 (2007): 22-30.

[7]. Rachidi, Farhad, et al. "A review of current issues in lightning protection of new-generation wind-turbine blades." *IEEE Transactions on Industrial Electronics* 55.6 (2008): 2489-2496.

[8]. Iosseli, A. S. Kothanof, M. G. Stlyrski, Calculation of capacitances (Moscow: Electric Power Press,1987, 24-30)

[9]. C. R. Paul, Inductance-loop and partial (NJ: John Wiley & Sons, Inc., 2010, 236-239)

[10]. Wang, Guozheng, et al. "Integrated multiple wave impedance model of offshore wind turbine considering blade rotation angle." 2016 *IEEE International Conference on High Voltage Engineering and Application (ICHVE). IEEE*, 2016.

[11]. Hosseini, SM Amin, Amir Mohammadirad, and Amir Abbas Shayegani Akmal. "Surge analysis on wind farm considering lightning strike to multi blade." Renewable Energy (2021).

[12]. Zhao, H. X., and Xiao-rong Wang. "Overvoltage analysis of wind turbines due to lightning stroke." Power System Technology 28.4 (2004): 27-29.

[13]. P. L. Kalantrof, L. A. Ceitlin, Manual of inductance calculation (Moscow: Electric Power Press,1992, 3-10)

[14]. Das, J. C. Transients in electrical systems. McGraw-Hill Professional Publishing, 2010.

[15]. A. Juan, Martinez-Velasco, Ed., Power systems transients parameter determination, 1st ed CRC Press Taylor & Francis Group, 2010.

[16]. Gustavsen, Bjørn. “Panel Session on Data for Modeling System Transients Insulated Cables,” In Power Engineering Society Winter Meeting, 2001. IEEE, vol.2, pp. 718-723.

IEEE, 2001.
[17]. Gudmundsdottir, Unnur Stella, Bjørn Gustavsen, Claus Leth Bak, and Wojciech, Wiechowski. “Field Test and Simulation of a 400 kV CrossBonded Cable System,” Power Delivery, IEEE Transactions on 26, no. 3 (2011): 1403-1410.
[18]. BS EN, “Conductors of insulated cables. BS EN 60228:2005.”
[19]. New.abb.com. 2021. ABB. [online] Available at: <https://new.abb.com/docs/default-source/ewea- doc/xlpe-submarine-cable-systems 2gm5007.pdf> [Accessed 21 November 2021].
[20]. Zhang, Li, et al. "Studies on an electromagnetic transient model of offshore wind turbines and lightning transient overvoltage considering lightning channel wave impedance." Energies 10.12 (2017): 1995.
[21]. Zhang, B.; Xue, H.Z.; Jin, Z.S. Transient Potential Distribution of Transmission Tower and Its Grounding Device under Lightning. High Volt. Eng. 2013, 39, 393– 398.
[22]. Wu, Zhi-liang, and Feng-wu Wang. "Blower foundation type in marine wind electric field and calculation method." *Port & Waterway Engineering* 10 (2008).
[23]. Pan, W. X., et al. "Grounding computation method for layered-soil with arbitrary massive texture foundation." *J. Transactions. of China Electro Technical. Society*, vol. 31, no. 7, pp. 145-151, Apr. 2016.
[24]. Paulino, Jose Osvaldo S., Wallace C. Boaventura, and Celio Fonseca Barbosa. "An approximate expression for the equivalent resistivity of a two-layer soil." Lightning Protection (XII SIPDA), 2013 International Symposium on. IEEE, 2013.
[25]. Nenghong, Xia, Lu Heng, and Qian Chao. "The Integrated Electromagnetic Transient Model of Wind Turbine Considering the Grounding Environment in Intertidal Zone." 2019 *IEEE 2nd International Conference on Electronic Information and Communication Technology (ICEICT). IEEE*, 2019.

**Mohamed A. Abouelatta** is currently an Associate Professor in the Electrical Power and Machine Department, Shoubra Faculty of Engineering, Benha University. He received his BSc, MSc, and PhD from Shoubra Faculty of Engineering, Benha University at 2001, 2005, and 2008, respectively. He is a member of the International Electrotechnical Commission team (IEC) in Egypt. His area of interest is study of electric and magnetic fields computations, electrostatic field effects of EHV lines on objects, partial discharge measurements and electrostatic separation technologies for fine granular mixtures, environmental pollution effects on HV insulators.

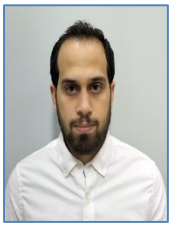

**Mahmoud Ezzat** was born in Cairo, Egypt, on May 27, 1994. He received the B.Sc. degree in Electrical Power and Machines with honour in 2017, Now he is studying his master’s degree in high voltage engineering from Electrical Power and Machines Department, Faculty of Engineering at Shoubra, Benha University, Cairo, Egypt. He is currently a teaching assistant with the Electrical Engineering department, Faculty of Engineering at Shoubra, Benha university. His research activity includes Transient Phenomenon in Power Networks and Renewable energy.

**Mousa A. Abd-Allah** was born in Cairo, Egypt, on August 16, 1961. He received the B.Sc. degree in electrical engineering with honor in 1984 and the M.Sc. degree in high voltage engineering in 1988, both from Zagazig University, Benha branch, Cairo, Egypt. He received the Ph.D. degree in high voltage engineering in 1992 from Cairo University. He is currently a Professor with the Electrical Engineering department, Faculty of Engineering at Shoubra, Benha University. His research activity include electromagnetic field assessment and mitigation, gas discharge in gas insulated systems, transient phenomenon on power networks, modern protection techniques of electrical power equipment.

**Abdelrahman Said** was born in Cairo, Egypt, on March 9, 1987. He received the B.Sc. degree in Electrical Power and Machines with honor in 2009, the M.Sc. degree in High Voltage Engineering in 2013, and the Ph.D. degree in High Voltage Engineering in 2016, all from Electrical Power and Machines Department, Faculty of Engineering at Shoubra, Benha University, Cairo, Egypt. He is currently a Associated Professor with the Electrical Engineering department, Faculty of Engineering at Shoubra,Benha university. His research activity includes: Transient Phenomenon in Power Networks, Artificial intelligent in power system, Renewable energy.